Разломо- и трещино-образование в коллекторах как результат локализации деформации: экспериментальный, теоретический, численный и геологический подходи

Mechanisms of deformation localization, fracturing, and faulting in reservoirs from experimental, theoretical, numerical, and field studies

Chemenda Alexandre I., Mas Daniel, Ambre Julien, Tran Huyen, Fan Jinyang, Petit Jean-Pierre, Bouissou Stéphane

V Балтийская школа-семинар
Петрофизическое моделирование осадочных пород

11-15 сентября 2016 года
г. Петергоф

Three (genetically different ?) object types

- Deformation localization bands
- Fractures (e.g., joints)
- Faults

- Geological Data
- Experimental Results
- Theoretical models
- Numerical Modeling

Natural examples:
1. Deformation bands

Pure compaction Bands

Pure compaction and shear-compactive Bands

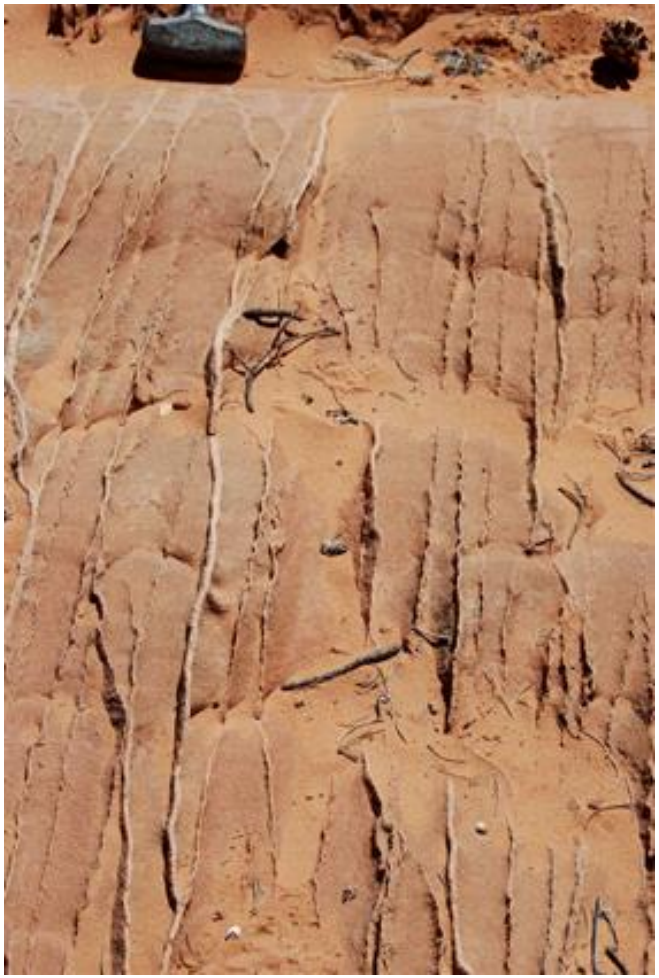

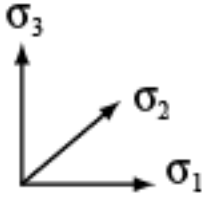

$\psi \approx 90°$ (Schultz at al.)

(Mollema and Antonellini, 1996, Schultz) $\psi \approx 90°$ $\psi \approx \pm 40°$

ψ is the angle between σ_1 and the deformation bands

$\psi \approx \pm 38°$

(Schultz, 2011)

Shear-Dilatant Bands/fractures, limestone

Maiella, limestone (L. Bazalgette)

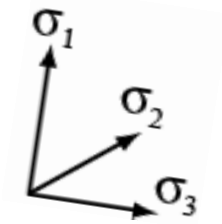

$\psi \approx \pm 18°$

Natural examples:

2. Faults

FAULTS, Shear Bands

Massif d'Urchaux, Southern France

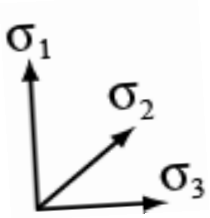

$\psi \approx \pm 25°$

(Wibberley et al.)

San Andreas Fault

Another fault type

LANDSLIDES

NW La Clapière landslide, Nice area, Southern France SE

Natural examples:

3. Joints

Diaclases = Joints

Bristol, limestone

$\psi \approx 0°$

Tasmania, sandstone

Plumose morphology of joint surfaces

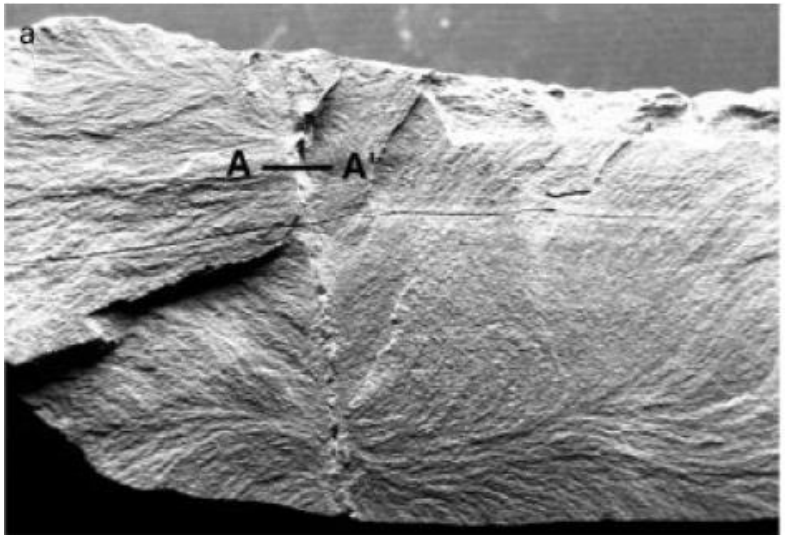

(McConaughy, Engelder, 2001)

The formation mechanism is believed to be Mode I (opening or tensile) fracturing

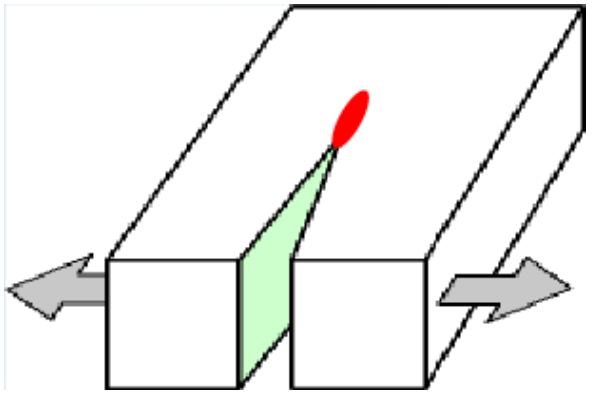

No joint opening is observed in many cases

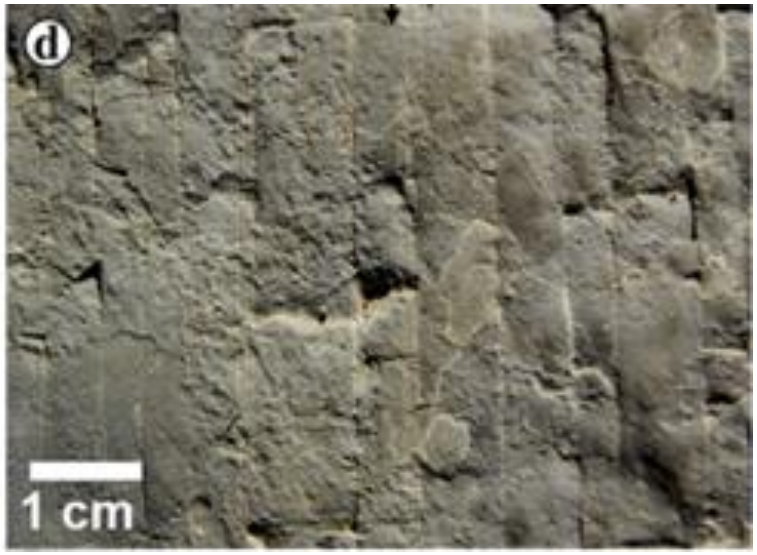

So what is the formation mechanism?

Geo-FracNet

Results of the experimental rock testing

Conventional (axisymmetric) tri-axial tests

Experimental Setup

Conventional triaxial press in Geoazur: General view

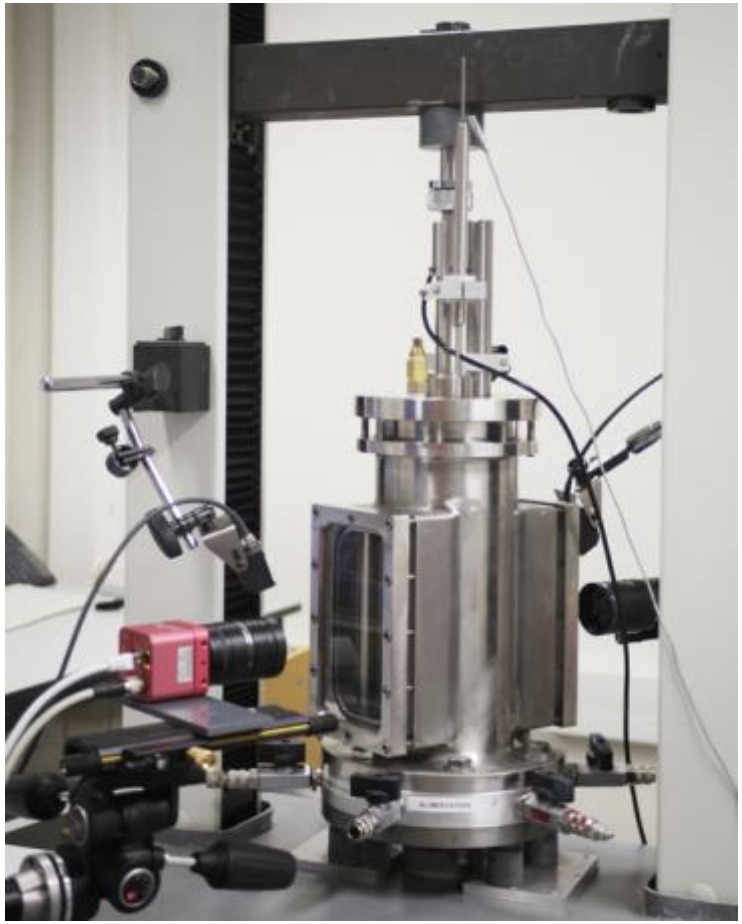

Conventional 3-axial compression and extension tests

Sample instrumented with LVDTs displacement gages for extension tests

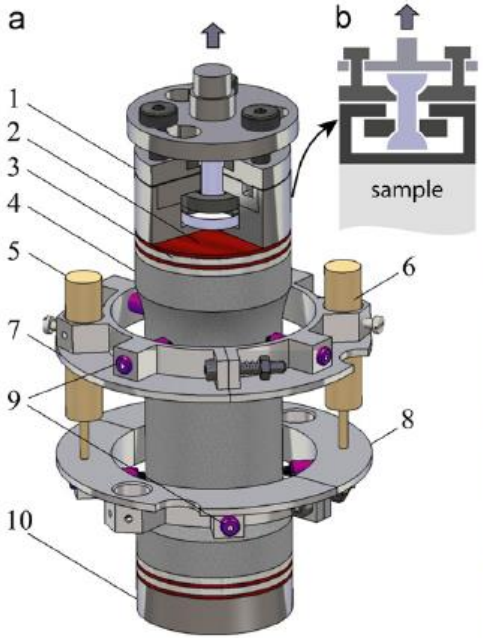

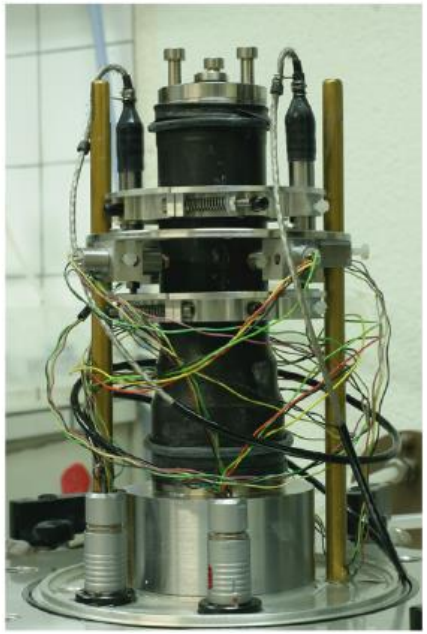

Axisymmetric compression tests: Lode angle $\theta = 60°$

GRAM1 samples fractured in Compression Tests

GRAM – Granular Rock Analogue Material

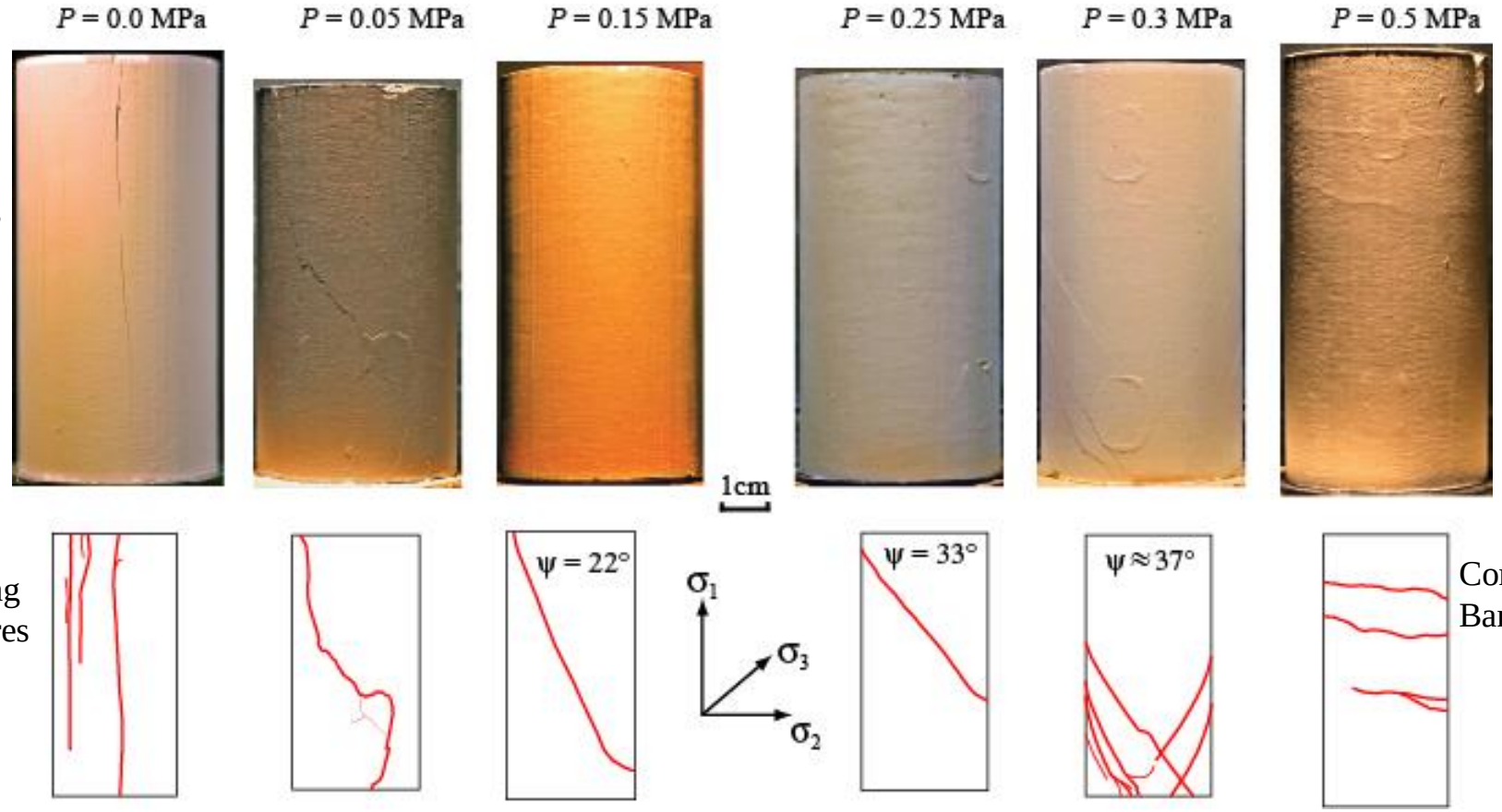

Grain size: ~0.3 µm

(Nguyen et al., *IJRMMS*, 2011)

Comparison of stress-strain curves for different materials

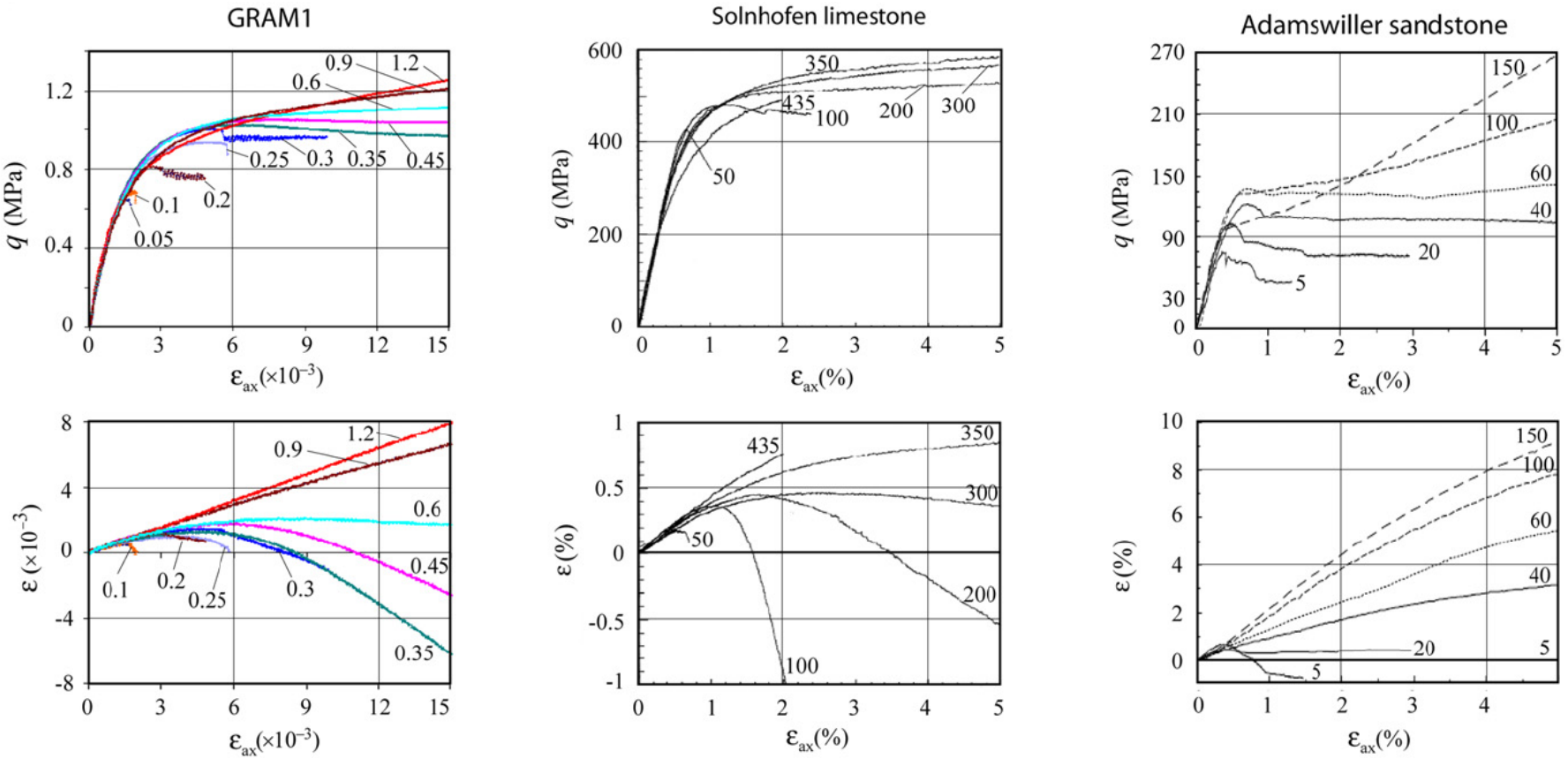

(Nguyen et al., *IJRMMS*, 2011)

Vosges Sandstone

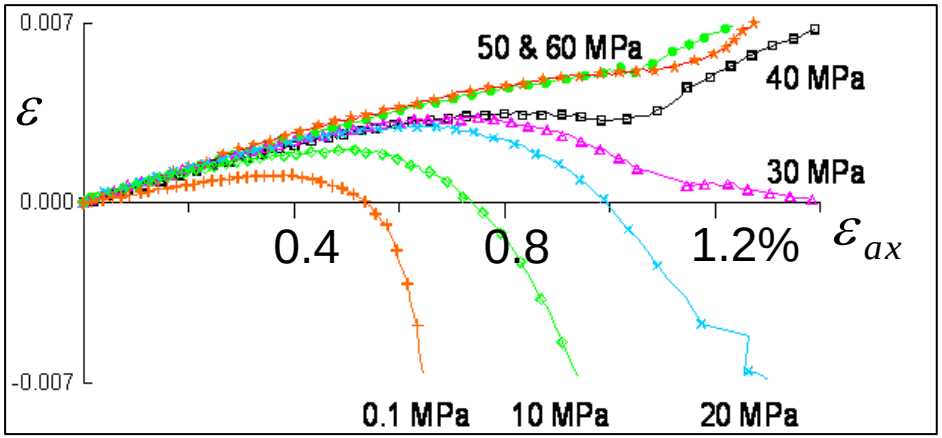

Conventional (axisymmetric) extension tests

Lode angle $\theta = 0°$

Conventional tri-axial Extension Tests: $\theta = 0^\circ$

σ_3-normal fractures (discontinuities)

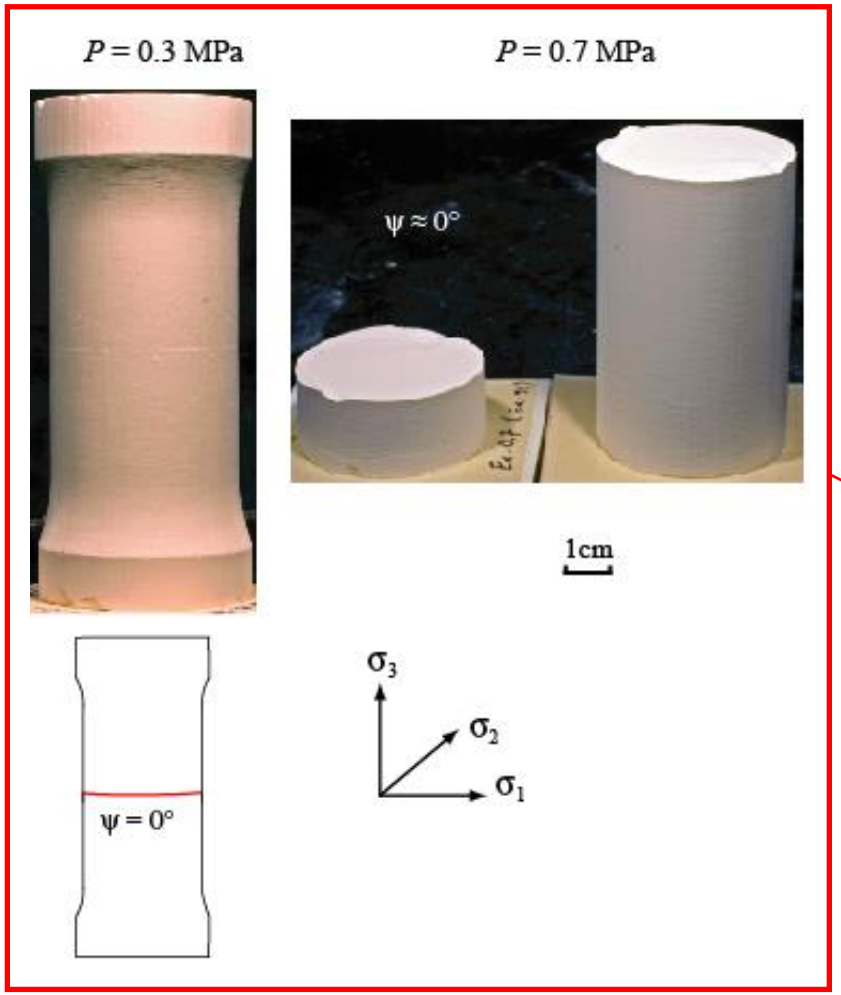

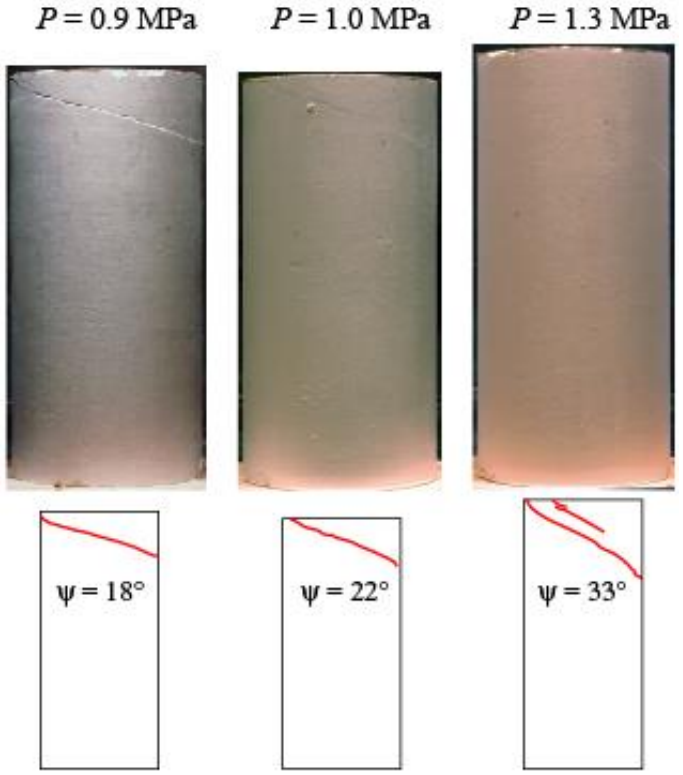

Compression Test: $\theta = 60^\circ$

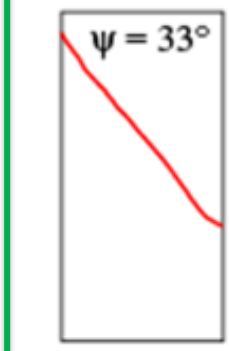

Axial stress at fracturing

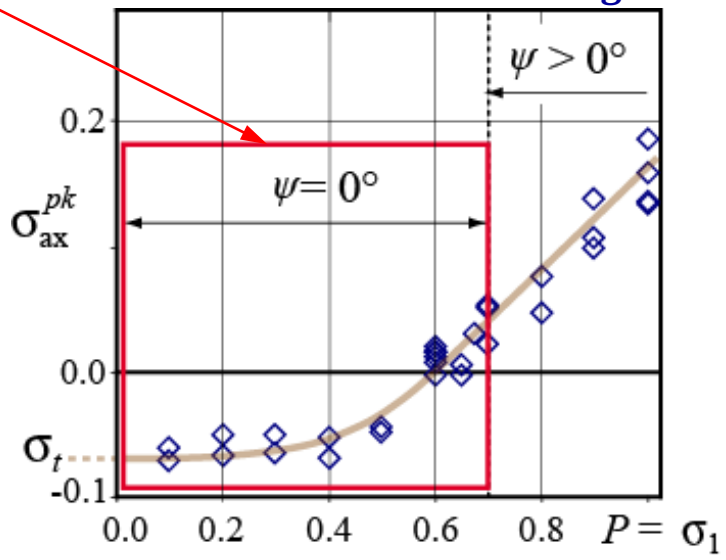

(Nguyen et al., *JRMMS*, 2011; Chemenda et al., *JGR*, 2011)

Surfaces of σ_3– orthogonal fractures generated in extension tests at different *P*

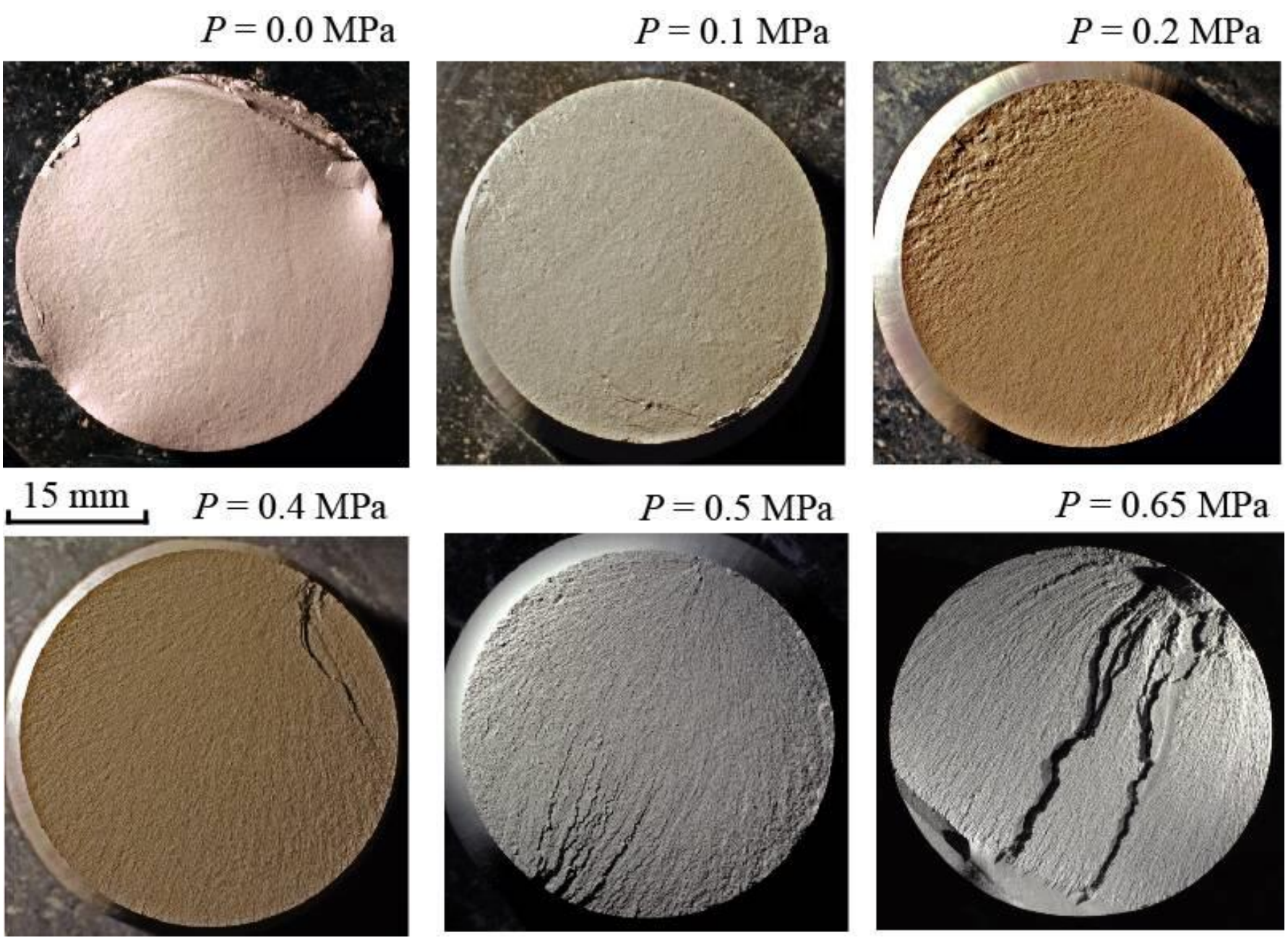

SEM image of the discontinuity (band) before its opening

P = 0.6 MPa

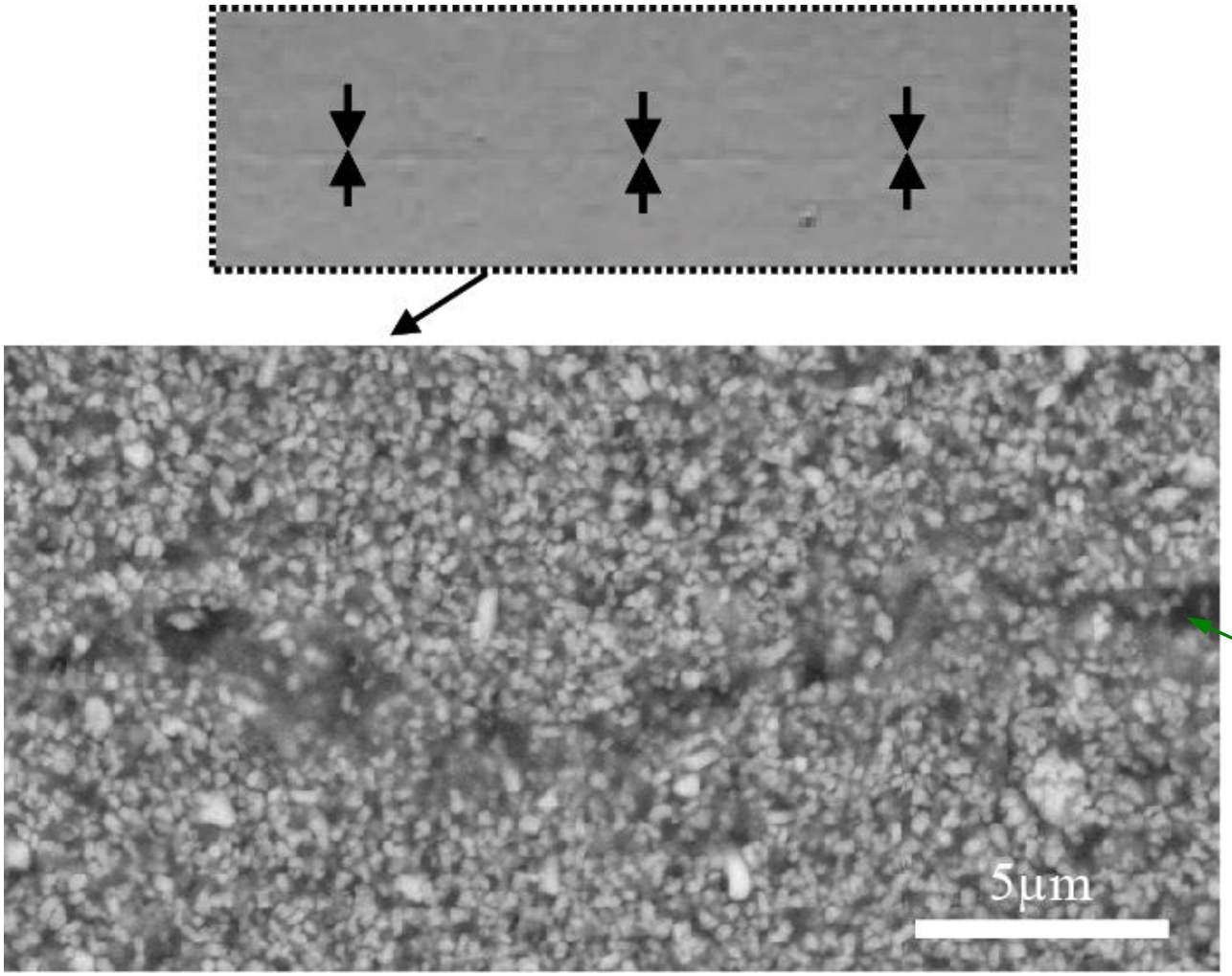

Transition from dilatancy banding to mode I cracking in GRAM with pressure reduction

$P = 0.1$ MPa

$P = 0.65$ MPa

Mode I fracture propagation resulting in smooth surfaces can occur only at very low effective mean stress

Fracture Surface in GRAM

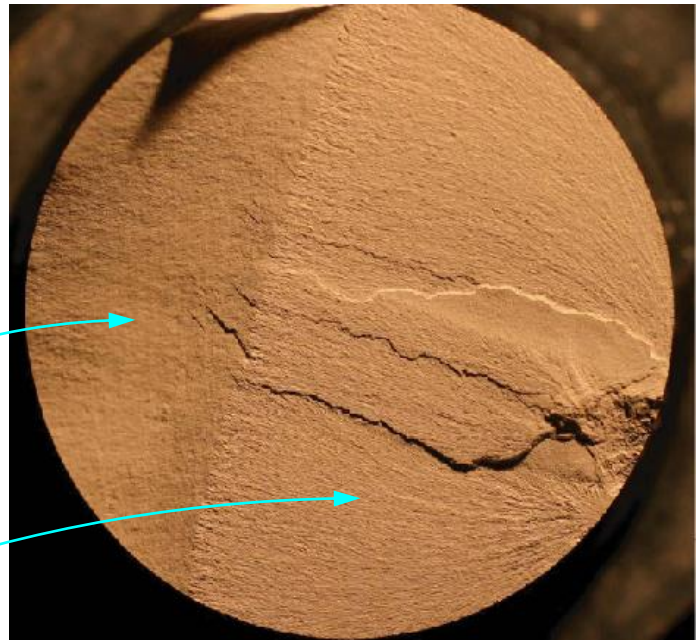

… in nature (pilite)

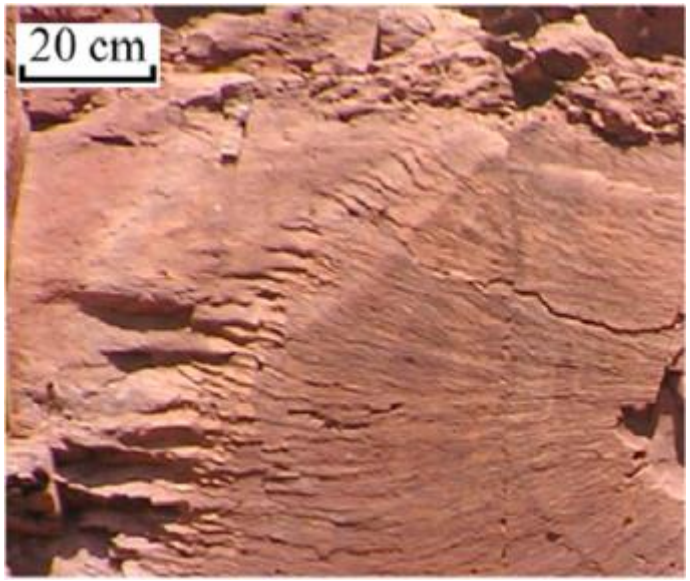

Microstructure of joints in dolomicrite

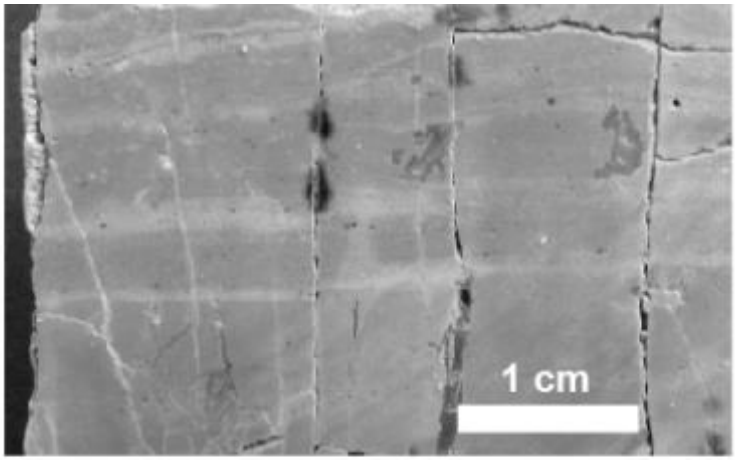

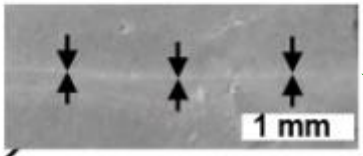

Embryonic joint

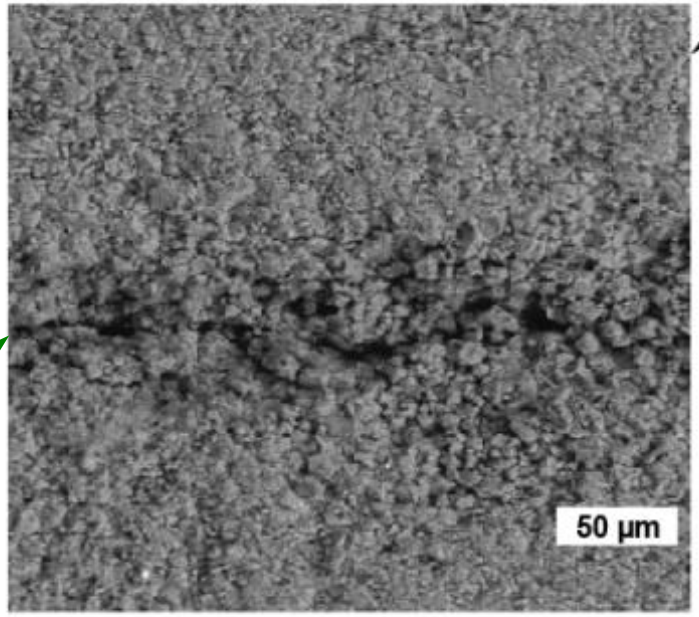

Dilatancy Band

Mode I cracking

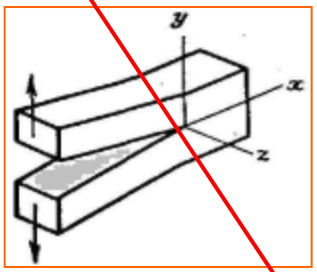

(Chemenda et al., CRAS, 2011)

Poly (true) 3-D tests

True 3-D GRAM tests

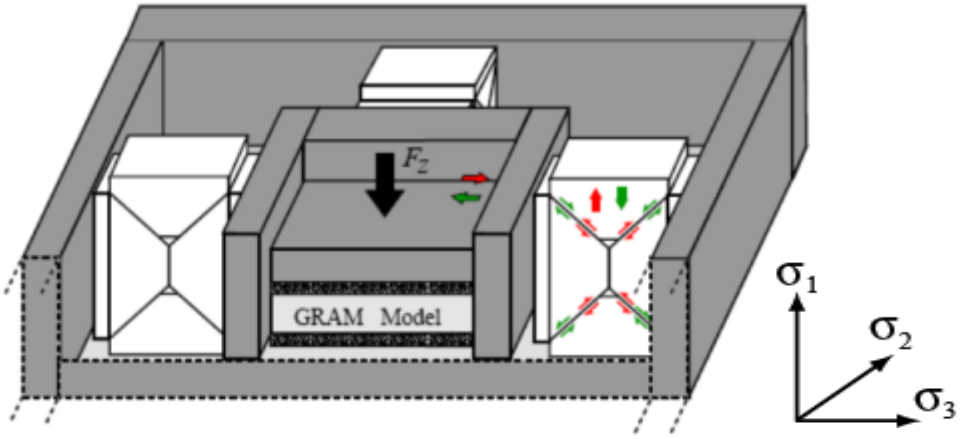

1cm

1cm

(Jorand et al., *Tectonophysics*, 2012)

NATURE

Limestone

(Engelder et al.)

GRAM physical/experimental models: True 3-D experiments

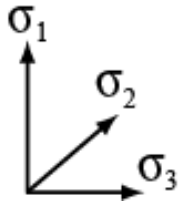

Continuity of the transition between different-type bands, suggesting the same/similar formation mechanism

Pressure increase

$\psi = 0 \rightarrow 9°$

Dilatancy bands (dilatancy joints)

$\psi = 14°$

Dilatant shear bands (rapidly evolve to shear fractures)

$\psi = 20°$

Pure shear bands/fractures

$\psi = 29°$

Compactive shear bands (never become fractures)

$\psi \rightarrow 90°$

$P = 0.5$ MPa

Pure compaction bands

(Jorand et al., 2012)

CONSTITUTIVE INSTABILITY

Rudnicki and Rice (*JMPS*, 1975):
Continuous Bifurcation

Localization of deformation corresponds to a loss of uniqueness of a boundary value problem and corresponds to the loss of ellipticity of the governing equations

Solution for the critical hardening modulus

(1) $$h(\alpha,\beta,N,\nu)=\frac{(1+\nu)\cdot(\beta-\alpha)^2}{9\cdot(1-\nu)}-\frac{1+\nu}{2}\cdot\left[N+\frac{1}{3}\cdot(\beta+\alpha)\right]^2$$

β – dilatancy factor; α –int. fric. coeff.; ν – Poisson's ratio;
h – hardening modulus; N – Lode-type stress-state parameter

Discontinuous Bifurcation:
Rice and Rudnicki (1980); Garagash (1981)

Chemenda (*JGR*, 2007):
Discontinuous Bifurcation

$$N=\frac{2}{\sqrt{3}}\cos\left(\frac{2\pi}{3}-\theta\right)$$

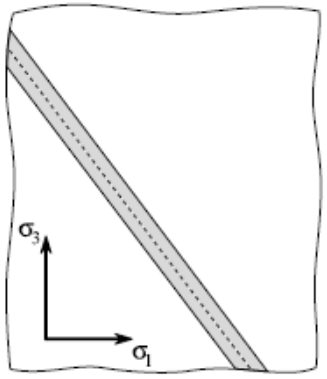

θ – Lode angle.

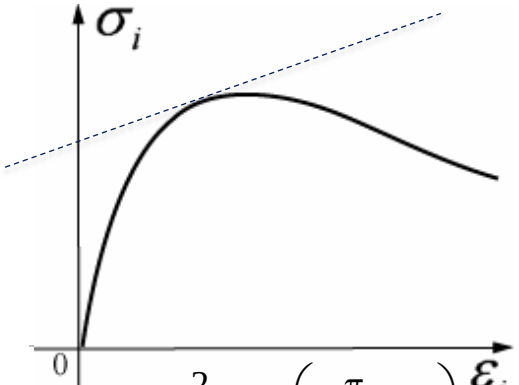

$$N(\theta):=\frac{2}{\sqrt{3}}\cdot\cos\left(2\frac{\pi}{3}-\theta\right)$$

$\chi=d/\lambda$ **At χ = 0, Eq. (2) is reduced to (1)**

χ – spacing parameter; d – band thickness; λ – band spacing.

(2) $$h(\alpha,\beta,N,\nu,\chi):=\frac{-1}{18}\cdot\frac{432.\cdot\nu\cdot\beta\cdot N+216.\cdot\nu^2\cdot\beta\cdot N+288.\cdot\nu\cdot\beta\cdot\alpha+360.\cdot\nu^2\cdot\beta\cdot\alpha-648.\cdot\chi-648.\cdot\chi^2+216.\cdot\nu^2\cdot\alpha\cdot N+432.\cdot\nu\cdot\alpha\cdot N+648.\cdot\nu\cdot N^2+36.\cdot\beta^2-324.\cdot N^2}{}$$

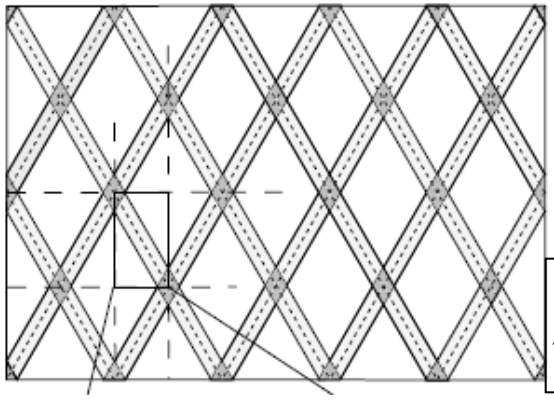

Orientation ψ of the bands in the stress space

$$\cos 2\psi=\frac{2(1+\nu)(\alpha+\beta+3N)-9N}{3\sqrt{4-3N^2}}$$

$$N=-s_2/\bar{\tau}$$

$$-1/\sqrt{3}\le N\le 1/\sqrt{3}$$

$N=1/\sqrt{3}$ Axisymmetric extension
$N=-1/\sqrt{3}$ Axisymmetric compress.

$$\beta=\frac{\dot{\varepsilon}^p}{\dot{\gamma}^p}=\frac{rate\ of\ inelastic\ \ volumetric\ strain}{rate\ of\ inelastic\ \ shear\ strain}$$

$$h=\frac{\partial\bar{\tau}}{G\partial\gamma^p}$$

at $\sigma=const$

G is the shear modulus.

Constitutive description of the properties of geomaterials is a major problems

Real Yield Surfaces obtained by separation of elastic and inelastic strains

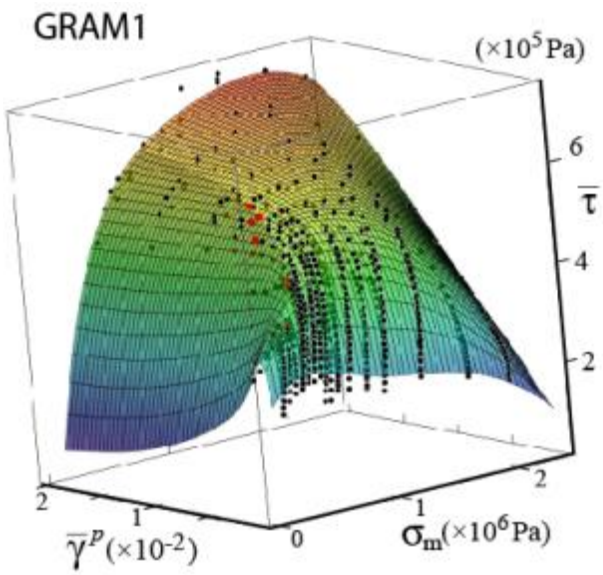

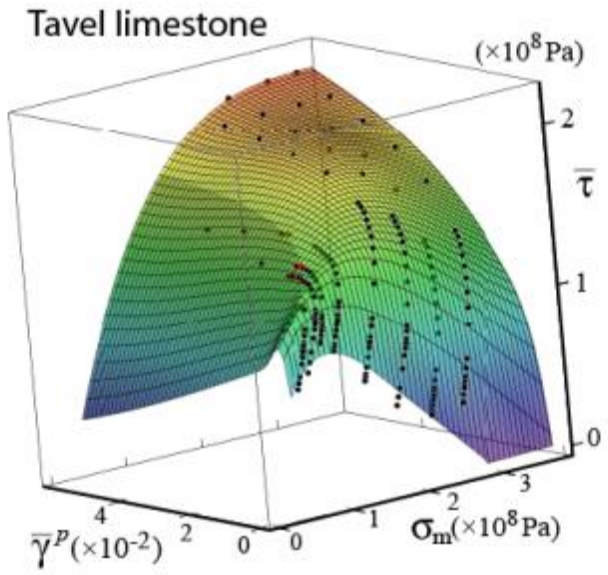

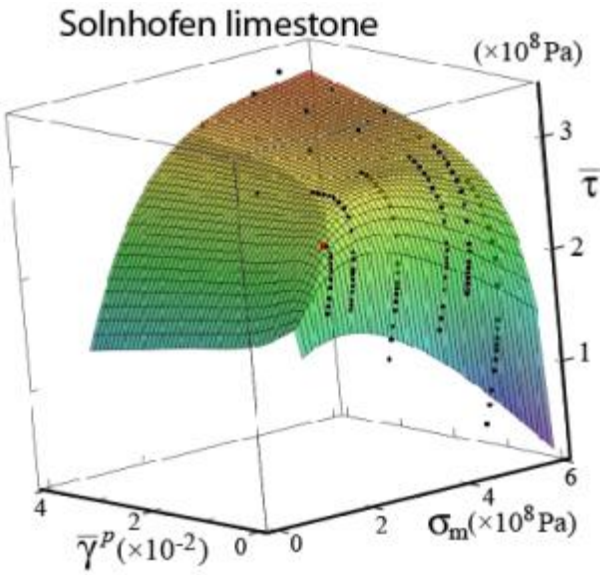

$\bar{\gamma}^p$ is the equivalent inelastic shear strain

Theoretical surface

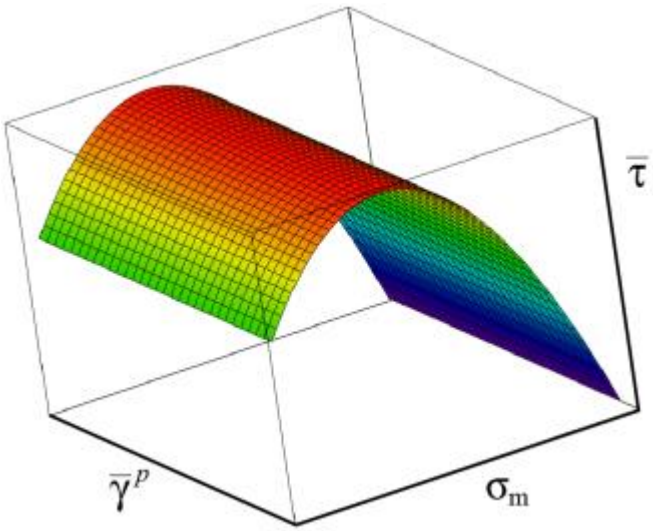

$$\alpha = \frac{\partial \bar{\tau}}{\partial \sigma_m}$$

$$H = \frac{\partial \bar{\tau}}{\partial \bar{\gamma}^p}$$

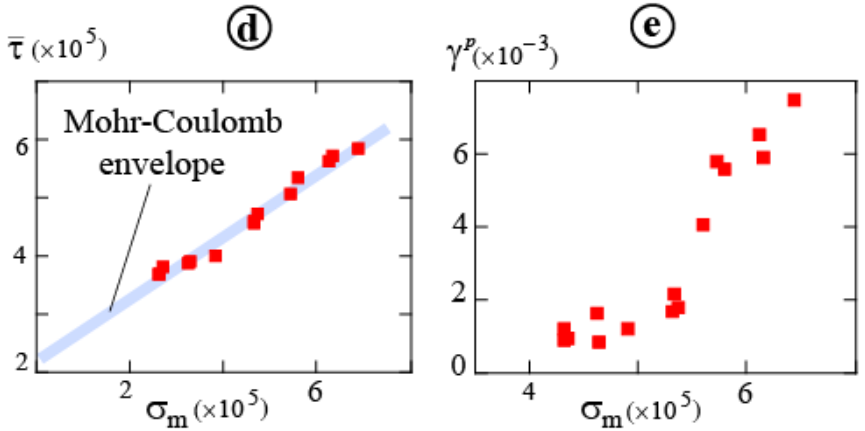

(Mas and Chemenda et al., 2015)

Evolution of the dilatancy factor β with the material damage (γ^p) and mean stress (σ)

$$\beta = \frac{\partial \varepsilon^p}{\partial \bar{\gamma}^p}$$

ε^p is the volume strain

GRAM1

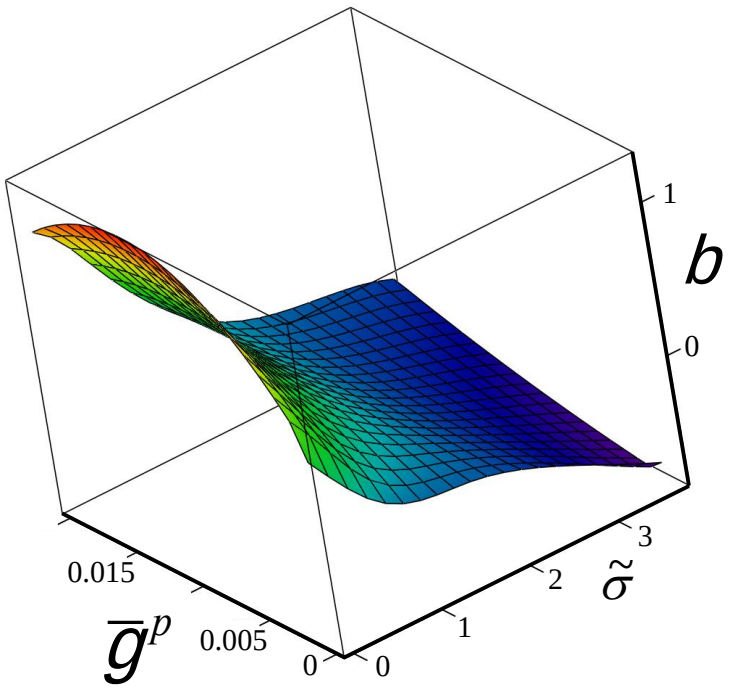

Tavel limestone

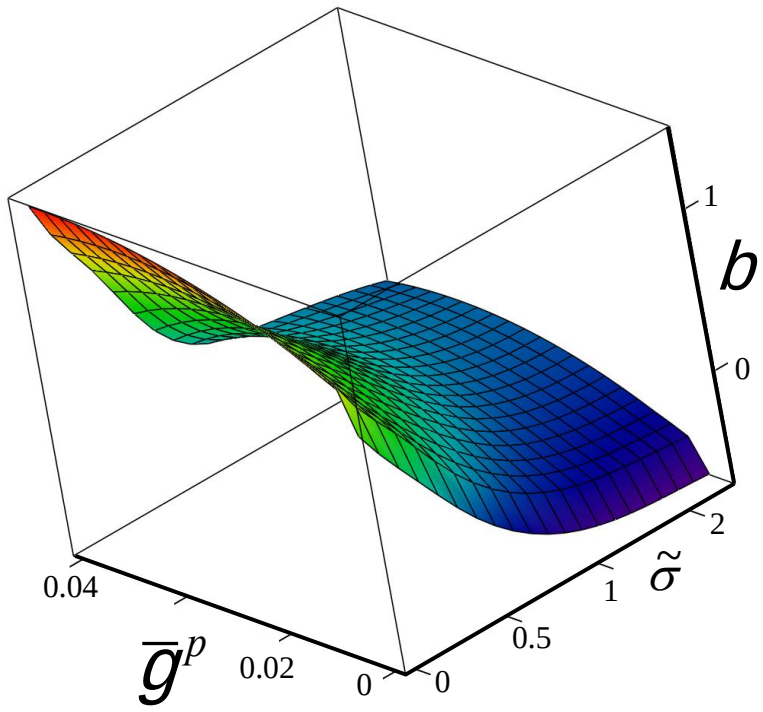

(Mas and Chemenda, *IJRMMS*, 2014)

Relation between internal friction coefficient α and dilatancy factor β

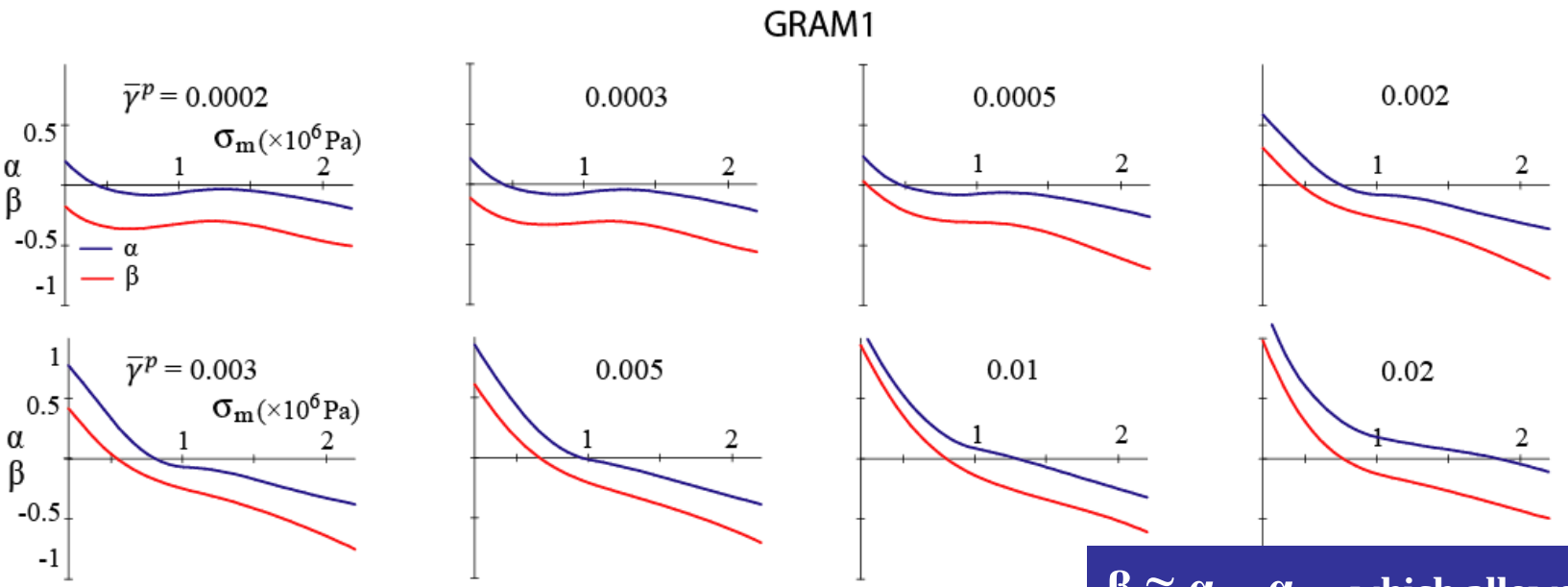

$\beta \approx \alpha - \alpha_0$, which allows relating the yield function and the plastic potential (Mas and Chemenda et al., 2015)

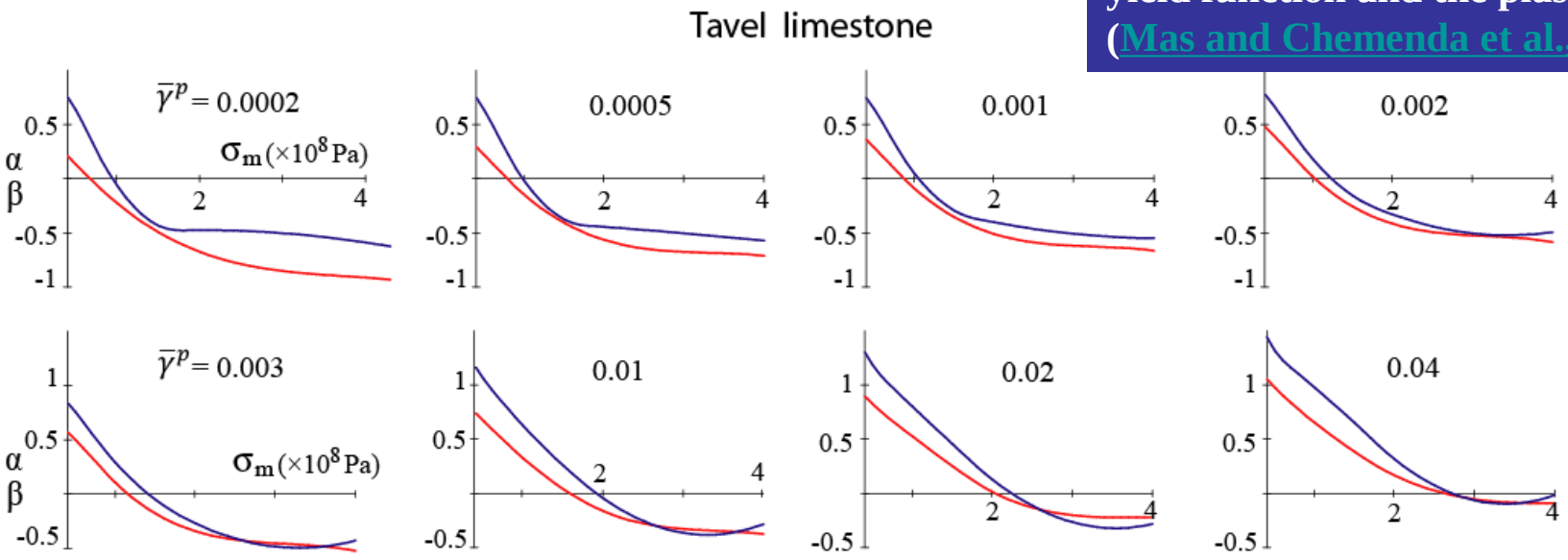

Numerical models:

1. Deformation bands/fractures

Orange, Southern France

Multi-strand structure of the bands

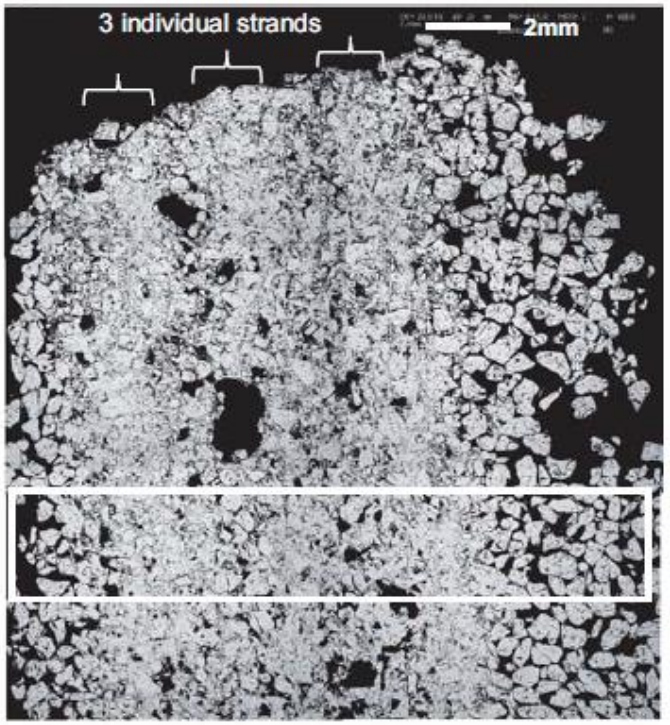

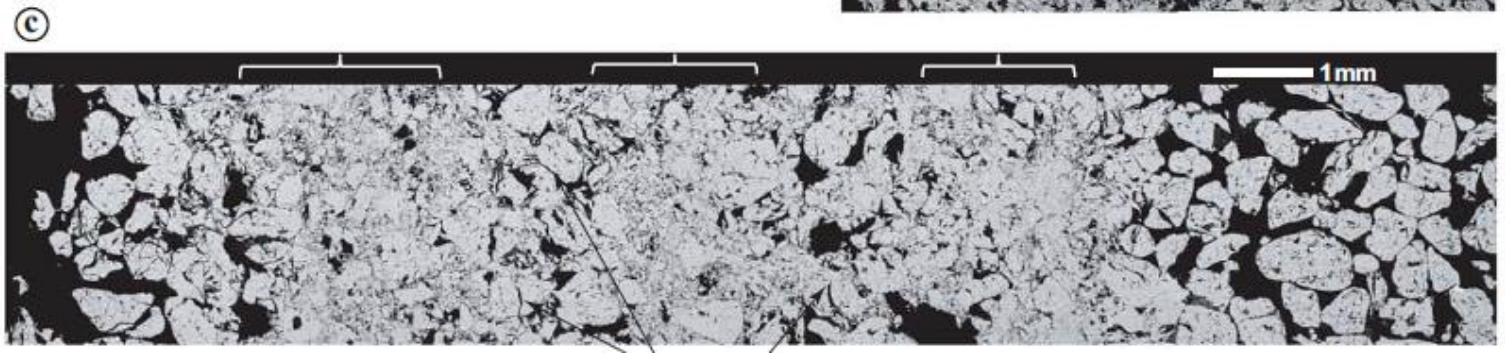

(Saillet and Wibberley, *JSG*., 2010)

Both the dilatancy factor and hardening modulus vary with deformation

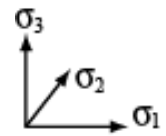

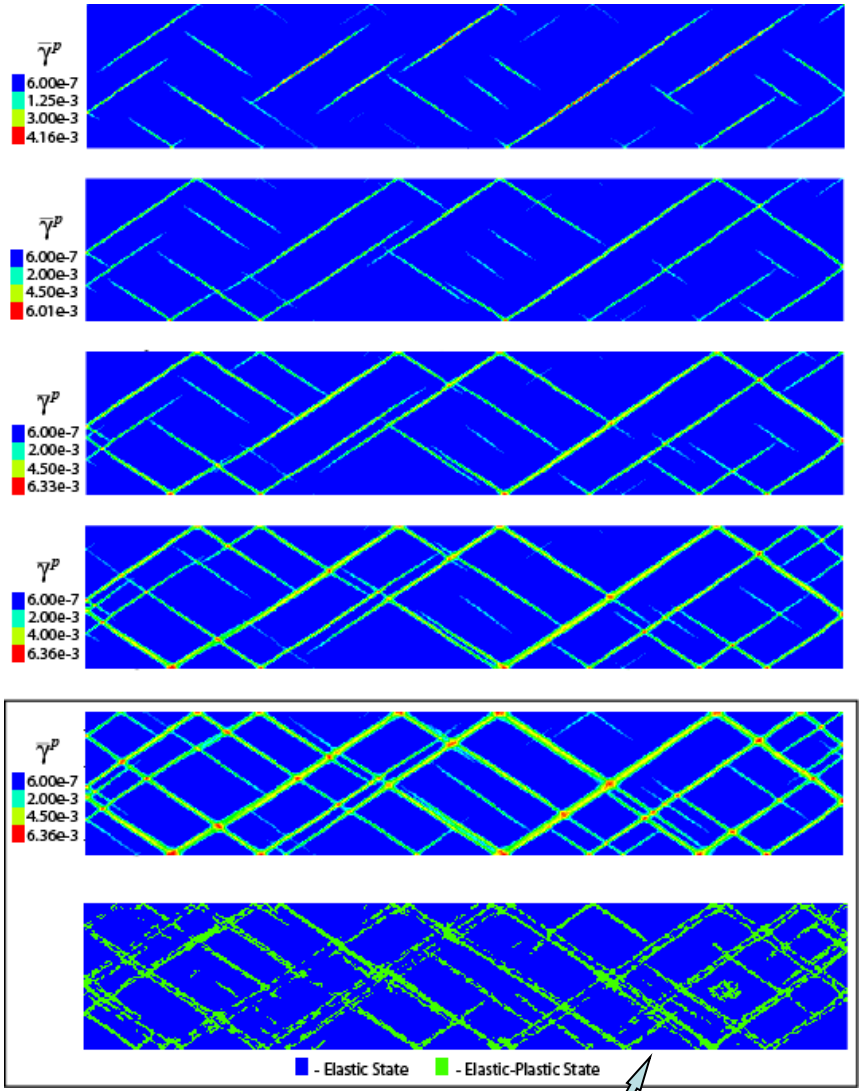

(Chemenda, Wibberley, Saillet, 2012)

Mechanical state

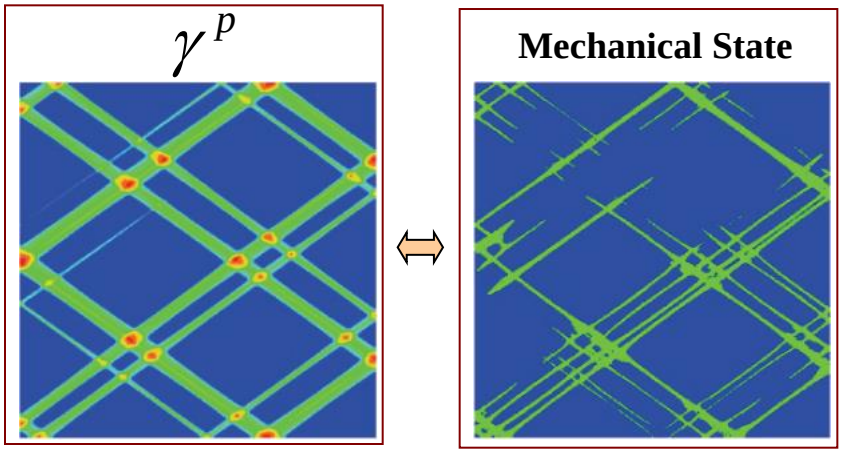

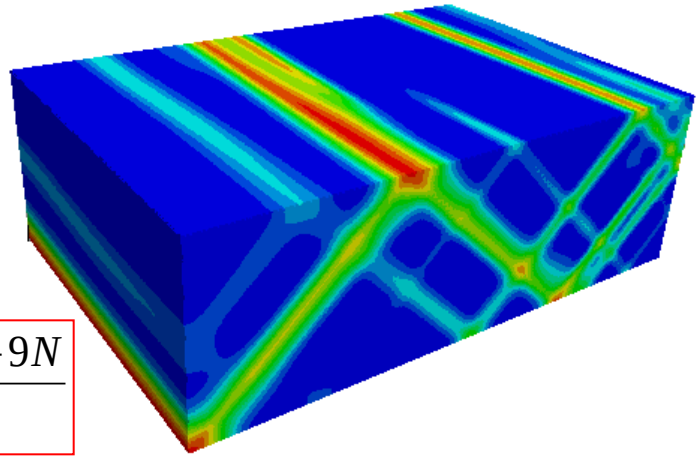

$$\cos 2\psi = \frac{2(1+\nu)(\alpha+\beta+3N)-9N}{3\sqrt{4-3N^2}}$$

FAULTS, Shear Bands

Massif d'Urchaux, Southern France

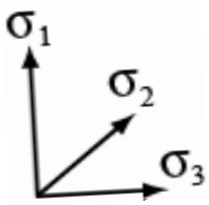

$\psi \approx \pm 25°$

(Wibberley et al.)

Numerical Model of Riedel-type experiment

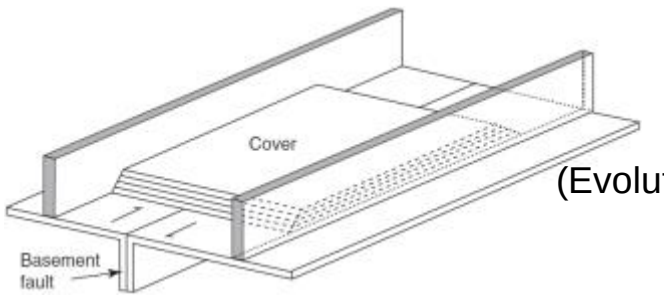

Model Setup

Elastoplastic model (plate) is deformed due to the basal shear traction τ_{yz}

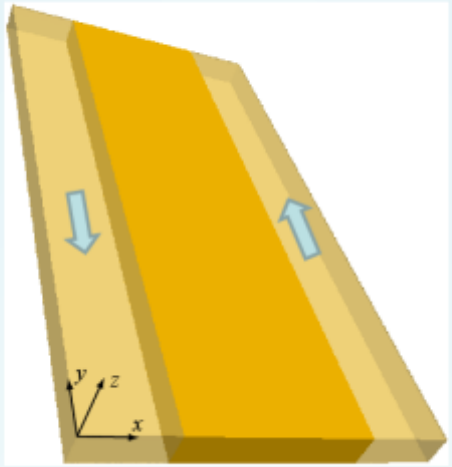

Basal shear traction τ_{yz} and initial displacement u_y profiles

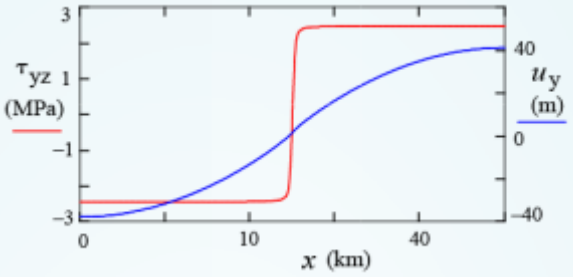

(Chemenda et al., 2016)

Evolution of deformation localisation and faulting

(Evolution of the accumulated equivalent inelastic strain (damage degree), γ^p, field)

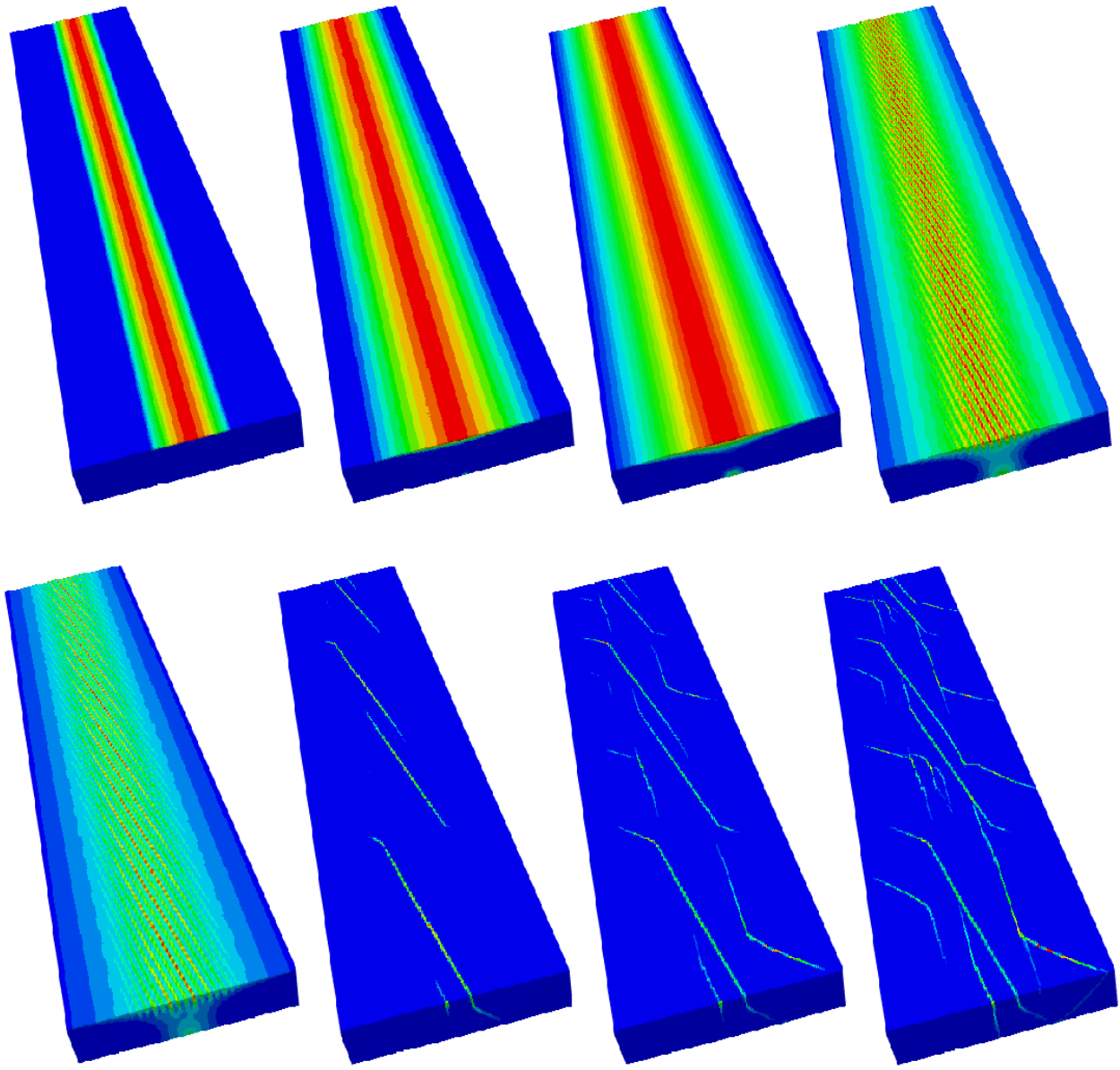

3-D architecture of the fault system

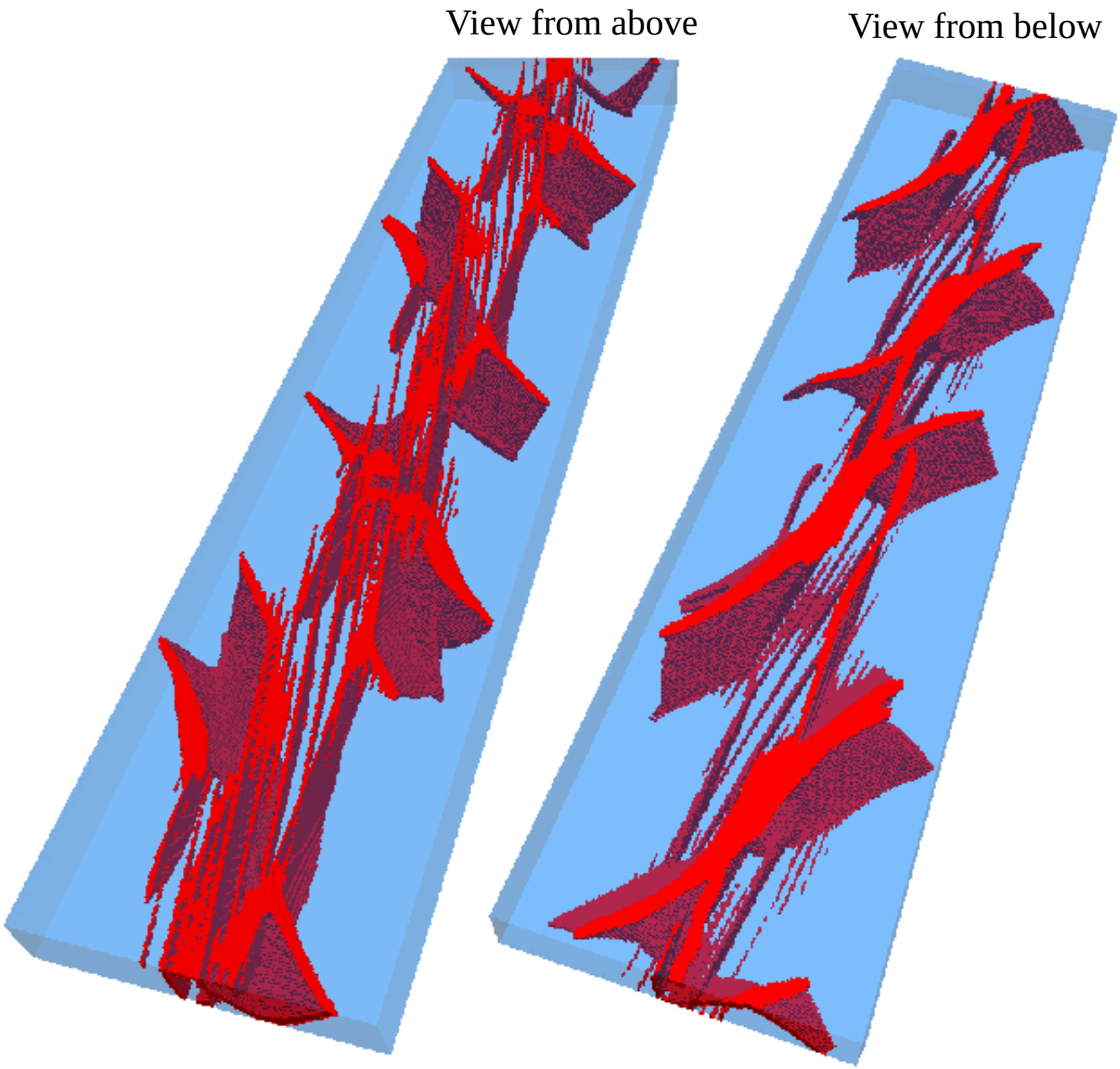

Comparison of the evolution of faulting in analogue and numerical models

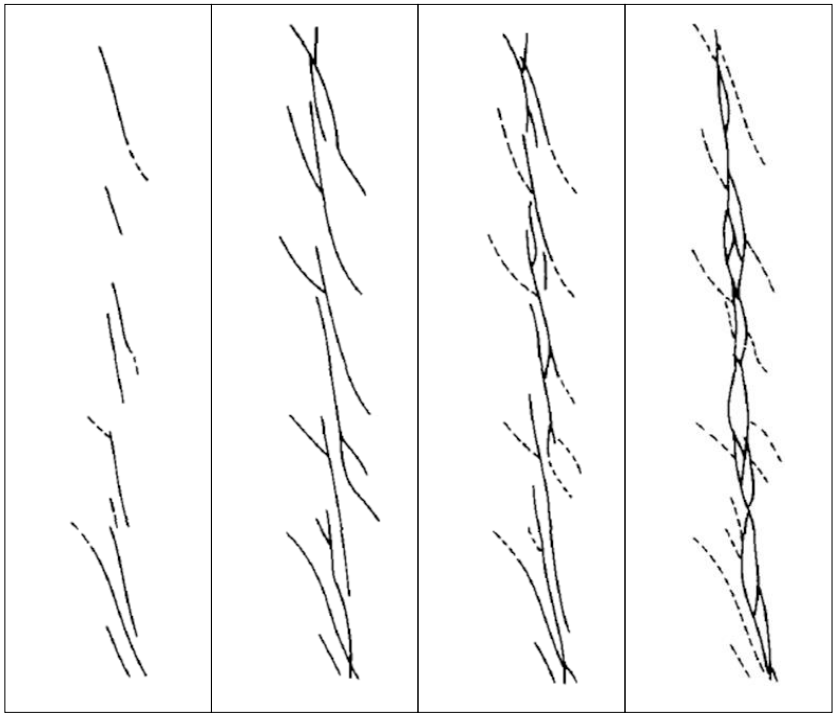

Sandbox model
(Naylor et al., 1986)

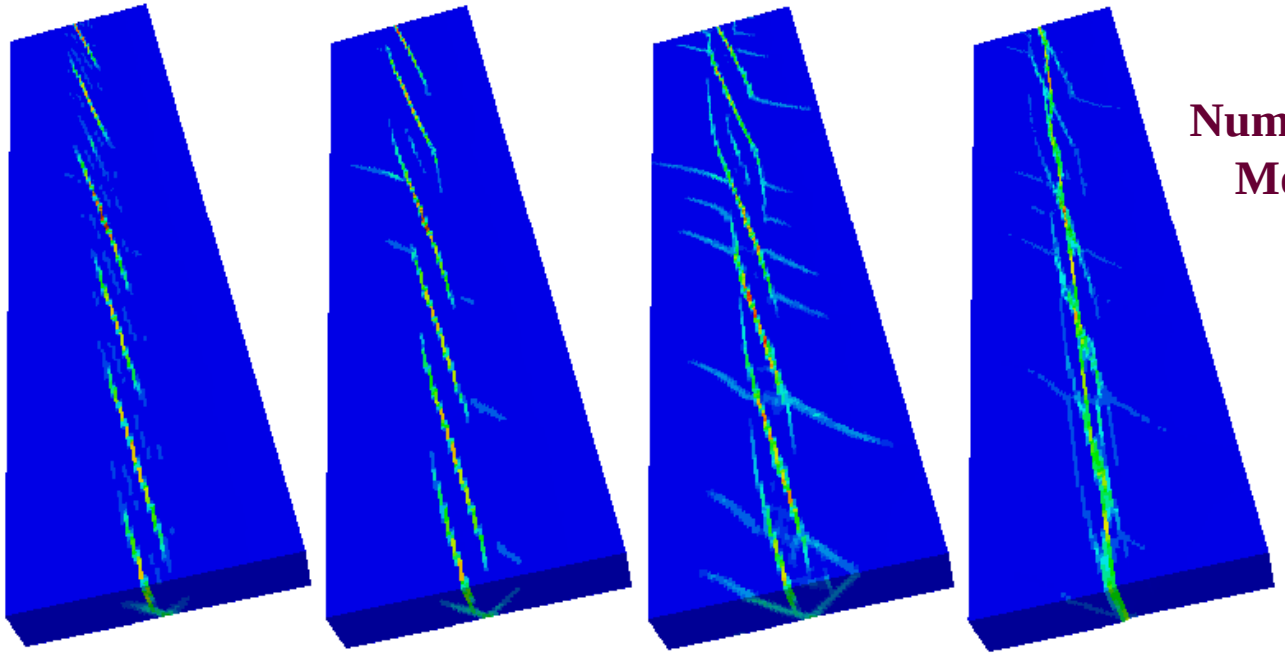

Numerical Model

Landsliding

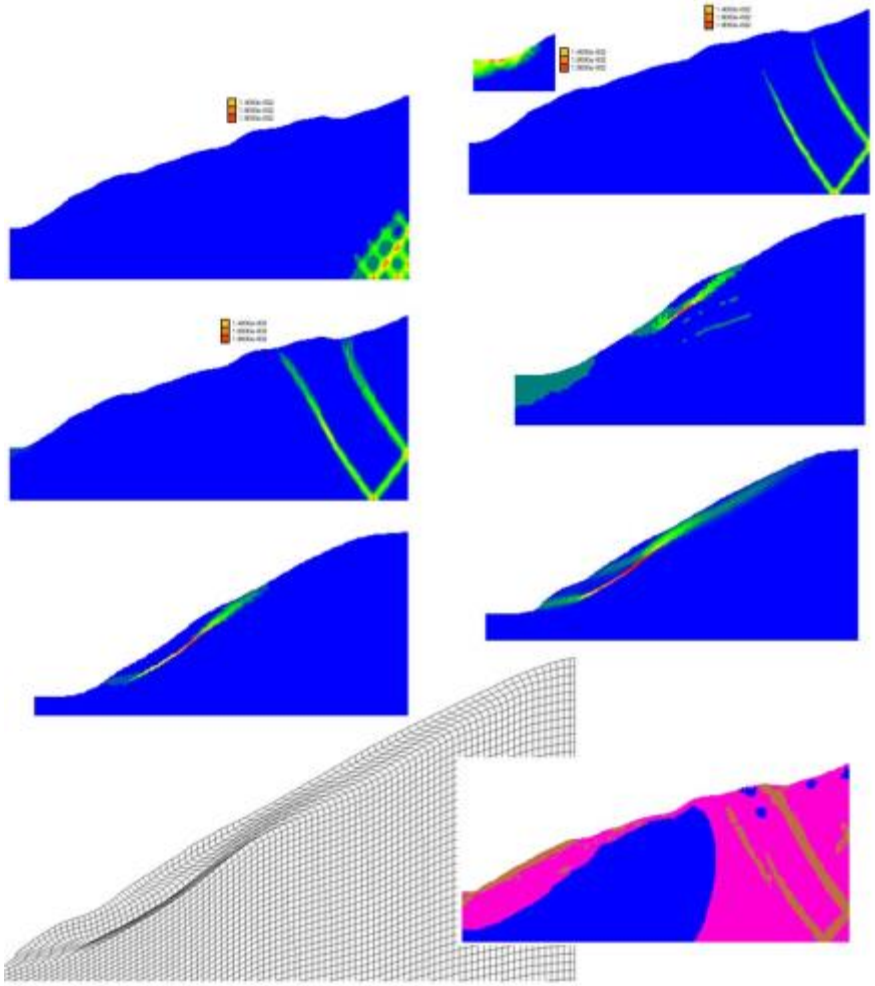

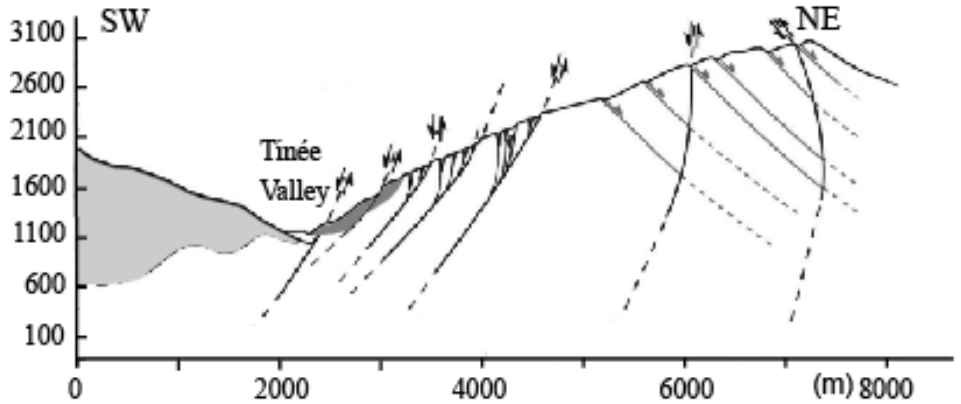

(Chemenda et al., 2009)

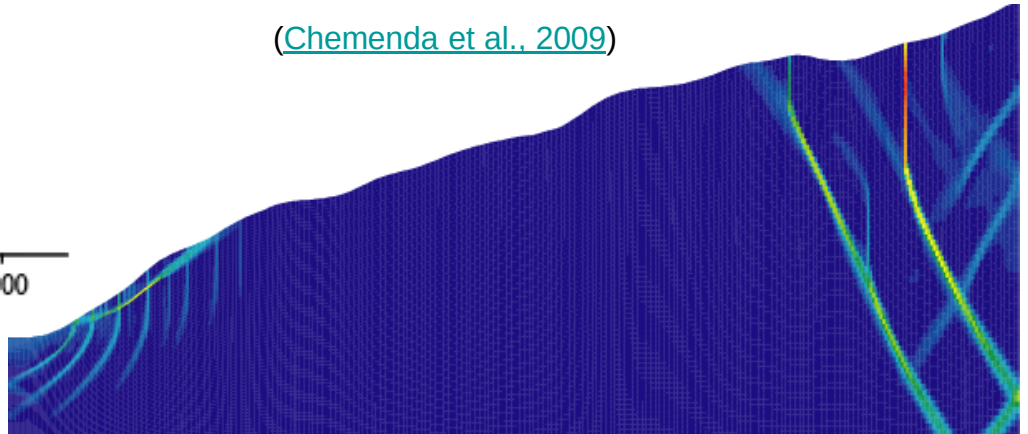

New Generation of Constitutive Models

taking into account all the 3 stress tensor invariants

Drucker-Prager model depends only on two stress tensor invariants, the mean stress (the 1st invariant) and the von Mises stress (the 2nd invariant). The influence of the 3rd invariant (that can be expressed in terms of the Lode angle θ) was believed to be negligible. Now it is clear that this is not generally true.

Journal of the Mechanics and Physics of Solids 96 (2016) 477–496

Contents lists available at ScienceDirect

Journal of the Mechanics and Physics of Solids

journal homepage: www.elsevier.com/locate/jmps

Dependence of rock properties on the Lode angle: Experimental data, constitutive model, and bifurcation analysis

Alexandre I. Chemenda *, Daniel Mas

Université Côte d'Azur, CNRS, OCA, IRD, Géoazur, 250 rue Albert Einstein, Sophia Antipolis, 06560 Valbonne, France

Initial yield envelopes for axisymmetric extension ($\theta = 0^o$) and compression ($\theta = 60^o$) for four materials

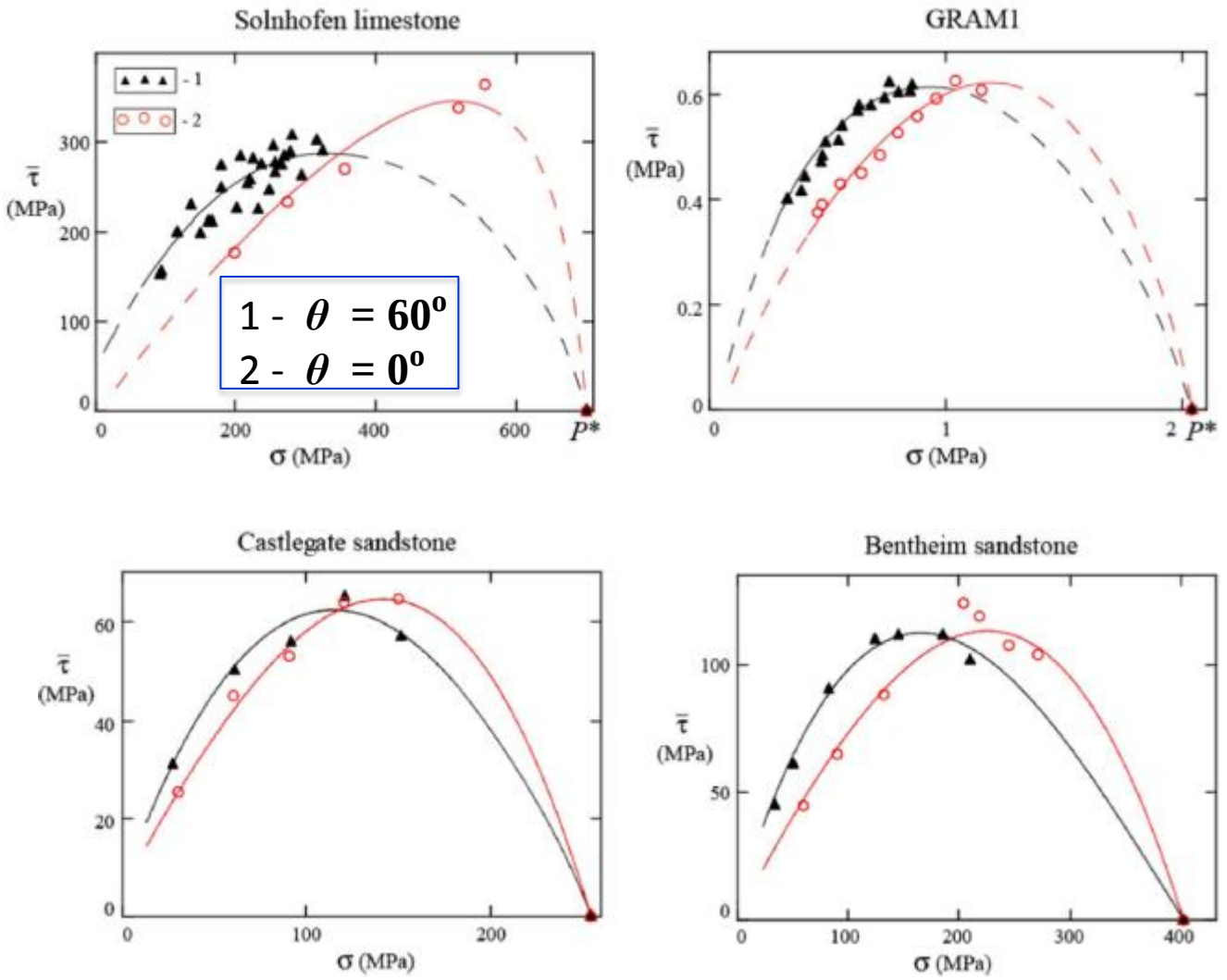

Yield surface for Castlegate Sandstone

Initial yield surface in the principal stress space and deviatoric plane

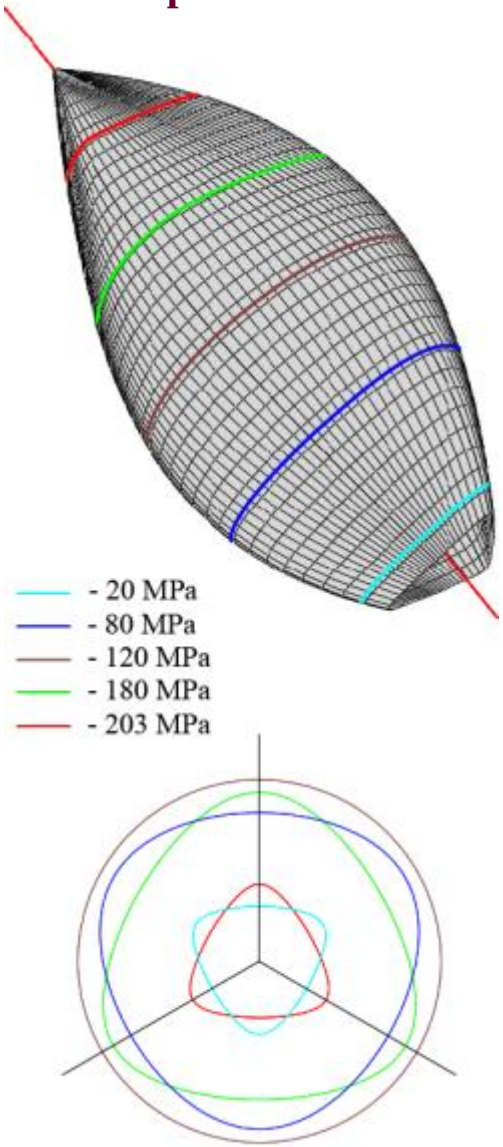

Deviatoric sections of the yield surface with the experimental points

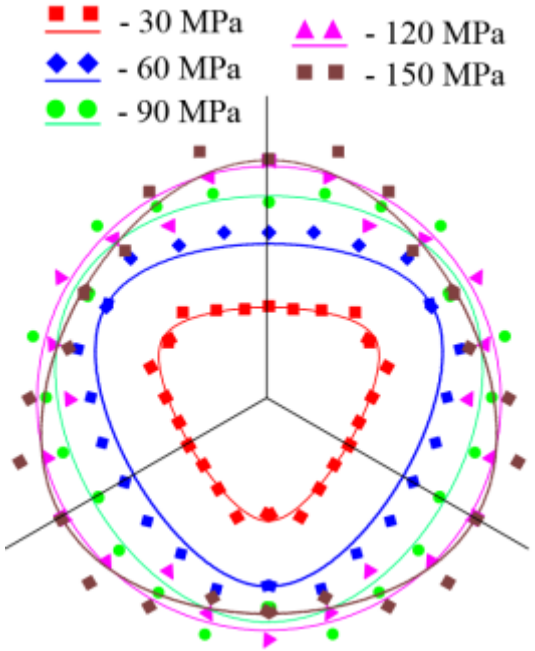

Dependence of the angle Ψ between the deformation band and σ_1 on the mean stress (σ) and the Lode angle (θ)

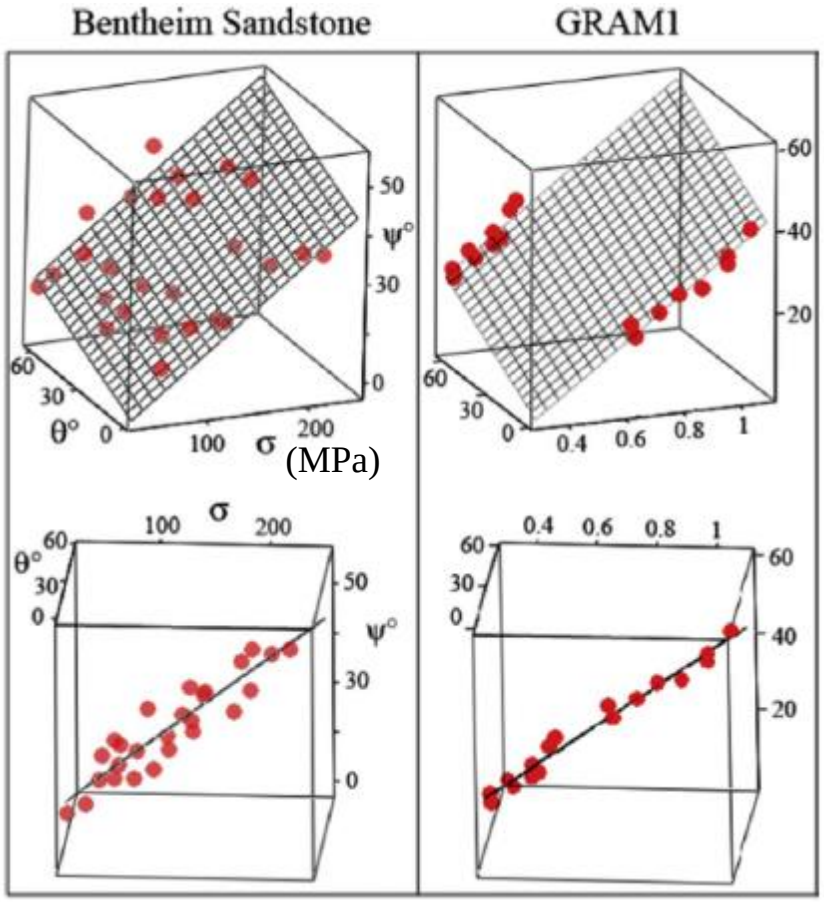

Ψ is ~10° larger for θ = 60° than for θ = 0° for the same σ

Brittle-ductile transition for θ = 0° occurs at σ ~1.5 times greater than for θ = 60°, meaning that at θ = 0° the material is more prone to fracture development

Dilatancy factor β as function of σ and θ

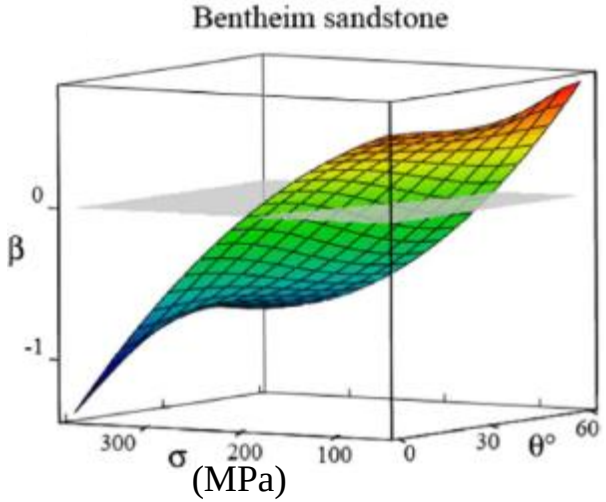

Dependence σ and Ψ at brittle-ductile transition on θ

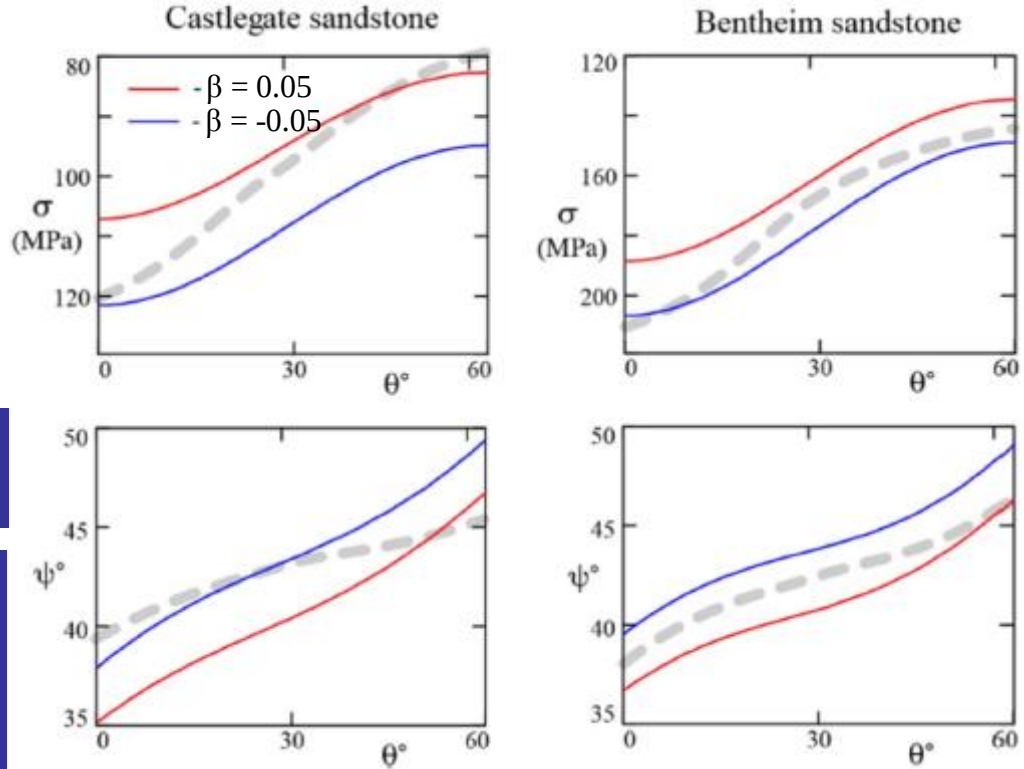

Dependence of the critical hardening modulus on σ and θ for 2 and 3-invariant constitutive models for Bentheim sandstone

New 3-invariant model

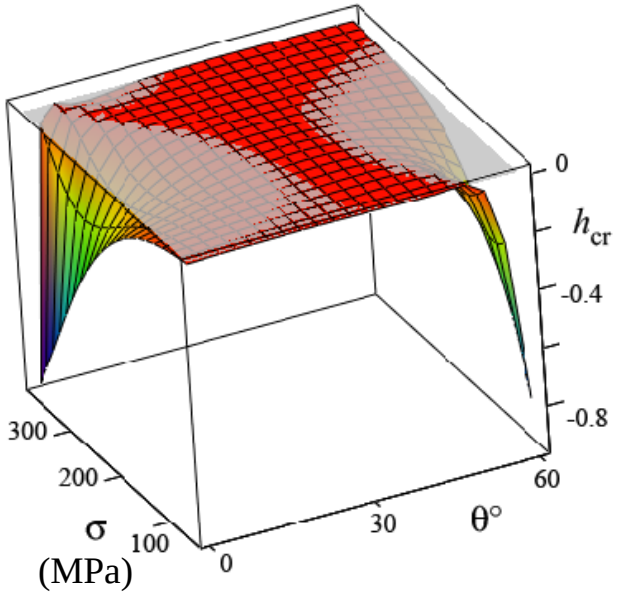

2-invariant Drucker-Prager model

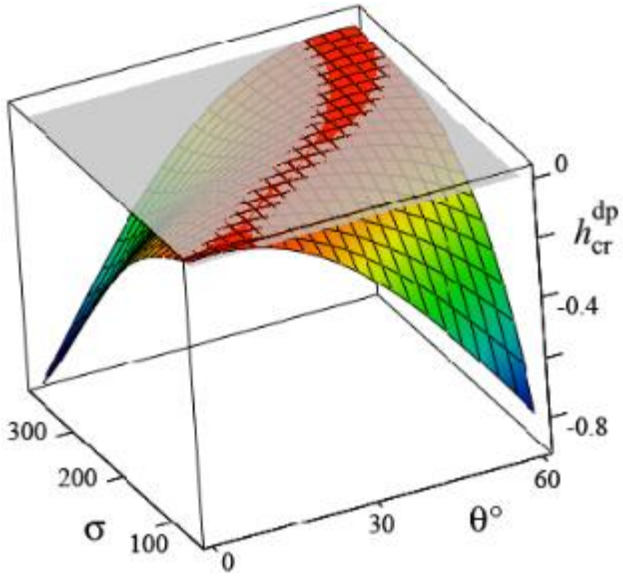

Difference between the two models

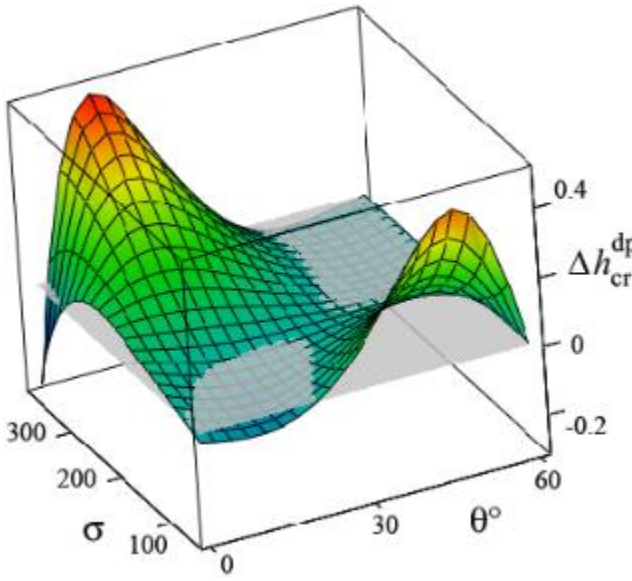

θ -dependence of rock properties encourages the strain localization and failure

The theoretical analysis of the proposed 3-invariant model shows that the parallelism of the failure (deformation localization) plane to the intermediate stress (σ_2) direction is no longer a "rule". This plane can considerably deviate from σ_2 , which seems to be confirmed by the experimental data (but more true 3-D experimental studies are necessary).

(Chemenda and Mas, *JMPS*, 2016)